On baroclinic instability in filtered and non-filtered numerical prediction models

By AKSEL WIIN-NIELSEN, *National Center for Atmospheric Research*

(Manuscript received November 19, 1962)

ABSTRACT

The criterion for baroclinic instability in a two level model of the large-scale motion in the atmosphere is computed and compared for the following cases: (1) A quasi-geostrophic model with constant static stability. (2) A quasi-geostrophic model with a horizontal variation of static stability. (3) A primitive equation model with constant static stability. (4) A primitive equation model with horizontal variation of static stability.

It is found that the models containing a horizontal variation of the static stability have a maximum instability at shorter wavelengths than the models with constant static stability; that only small differences are observed in the amplification rate of baroclinic disturbances in models with the same variation of static stability but with different basic equations as long as the variation of the meteorological parameters are in the observed range; but that large differences in the amplification rate occur when the Richardson number is small, i.e. for small mean static stabilities and/or large vertical wind shears.

The structure of the baroclinically unstable disturbances are computed and compared for the four models mentioned above. The variation of the ageostrophic wind and the static stability through the wave is of special importance. It turns out that the maximum ageostrophic wind at the upper level is about 15 % of the maximum wind, while the corresponding number at the lower level is 20 %. The distribution of the ageostrophic wind at the upper level is such that the wind is supergeostrophic around the ridge in the geopotential with a maximum close to the maximum geopotential and subgeostrophic around the trough in the geopotential. The distribution of static stability in the developing baroclinic wave is such that the air becomes more stable than the average between the ridge and trough (looking downstream), but more unstable between the trough and the ridge.

1. Introduction

The quasi-geostrophic models used in studies of short range numerical prediction schemes and studies of the general circulation of the atmosphere have been investigated in detail by theoretical methods and by application in numerical experiments, including operational forecasting. The performance of these models leaves something to be desired. Although the testing program of these quasi-geostrophic models or modifications thereof is still unfinished, there has recently been an increasing interest in the performance of the primitive equations. It seems, therefore, worthwhile to compare atmospheric models based upon the two systems of equations. In particular, one is able to investigate the magnitude of the meteorological parameters which are left out in the quasi-geostrophic equations in their simplest form, as for instance the ageostrophic wind-components.

Lorenz (1960) has recently shown in which way it is possible to formulate a two-layer model with a horizontal variation of static stability. This model has been analyzed in its simplest form by Gates (1961*b*), who was especially interested in the baroclinic instability inherent in this model and in the energy transformations. Lorenz' approach, which is possible because of a special application of the thermodynamic equation, can also be applied to the primitive equations. We can, therefore, generalize the balanced models with and without variation of static stability to models based upon the primitive equations. Since Gates (loc. cit.) has already compared the two balanced models we need not be concerned with this comparison here.

The comparison between the different models will, for simplicity, be restricted to the two-layer models in this paper. We shall furthermore only be concerned with the linearized versions of the equations on the beta-plane. The beta-plane approximation can probably only be justified rigorously for atmospheric motions whose scale is small compared to the radius of the earth. We shall nevertheless extend our calculations to scales where this criterion is not fulfilled. The reason for this procedure is that we might find tentative results which can later be investigated using a less restrictive geometrical system and the non-linear equations.

The comparison between the different systems will first of all be done by computing the linear baroclinic instability criterion. However, when the real and imaginary part of the phase speed are known we are also in a position to determine the amplitude and phase of all parameters entering the problem except one, which must be prescribed in an arbitrary fashion. In this way we can determine the structure of the different waves, in particular the amplifying baroclinic wave.

2. The basic models

We shall start this section by deriving the equations for the most general model of the four which we are going to consider. The complete system of equations which we are going to consider is:

$$\left.\begin{aligned}
&\frac{\partial u}{\partial t}+u\frac{\partial u}{\partial x}+v\frac{\partial u}{\partial y}+\omega\frac{\partial u}{\partial p}=-\frac{\partial \phi}{\partial x}+fv,\\
&\frac{\partial v}{\partial t}+u\frac{\partial v}{\partial x}+v\frac{\partial v}{\partial y}+\omega\frac{\partial v}{\partial p}=-\frac{\partial \phi}{\partial y}-fu,\\
&\frac{\partial \phi}{\partial p}=-\frac{R}{p}\theta\left(\frac{p}{p_0}\right)^{R/Cp}\\
&\frac{\partial u}{\partial x}+\frac{\partial v}{\partial y}+\frac{\partial \omega}{\partial p}=0,\\
&\frac{\partial \theta}{\partial t}+\frac{\partial \theta u}{\partial x}+\frac{\partial \theta v}{\partial y}+\frac{\partial \theta \omega}{\partial p}=0.
\end{aligned}\right\} \quad (2.1)$$

In (2.1) u, v and ω are the three velocity components in a coordinate system with pressure (p) as the vertical coordinate. ϕ is the geopotential, θ potential temperature, R the gas constant for dry air, c_p the specific heat for constant pressure, f the Coriolis parameter and p_0 a standard value of pressure ($p_0 = 100$ cb).

The first step in our procedure is to replace the two equations for the horizontal flow by the vorticity and the divergence equations. The first two equations in (2.1) are therefore changed to

$$\left.\begin{aligned}
&\frac{\partial \zeta}{\partial t}+u\frac{\partial \zeta}{\partial x}+v\frac{\partial \zeta}{\partial y}+\omega\frac{\partial \zeta}{\partial p}+\beta v=-(\zeta+f)\nabla\cdot\mathbf{v}\\
&\qquad\qquad+\frac{\partial u}{\partial p}\frac{\partial \omega}{\partial y}-\frac{\partial v}{\partial p}\frac{\partial \omega}{\partial x},\\
&\frac{\partial \nabla\cdot\mathbf{v}}{\partial t}+u\frac{\partial \nabla\cdot\mathbf{v}}{\partial x}+v\frac{\partial \nabla\cdot\mathbf{v}}{\partial y}+\omega\frac{\partial \nabla\cdot\mathbf{v}}{\partial p}\\
&\qquad\qquad+(\nabla\cdot\mathbf{v})^2+2\left(\frac{\partial v}{\partial x}\frac{\partial u}{\partial y}-\frac{\partial v}{\partial y}\frac{\partial u}{\partial x}\right)\\
&\qquad+\frac{\partial \omega}{\partial x}\frac{\partial u}{\partial p}+\frac{\partial \omega}{\partial y}\frac{\partial v}{\partial p}=-\nabla^2\phi+f\zeta\\
&\qquad\qquad+v\frac{\partial f}{\partial x}-u\frac{\partial f}{\partial y}.
\end{aligned}\right\} \quad (2.2)$$

We are next going to write the horizontal wind as a sum of the non-divergent and the divergent components, i.e.

$$\mathbf{v}=\mathbf{k}\times\nabla\psi+\nabla\chi. \quad (2.3)$$

Here ψ is the stream function and χ the velocity potential.

This means that the vertical component of vorticity and the divergence of the horizontal wind can be written:

$$\zeta=\nabla^2\psi, \quad \nabla\cdot\mathbf{v}=\nabla^2\chi. \quad (2.4)$$

The basic state on which the perturbations will be superimposed will be a zonal flow $U=U(p)$ which is a function of pressure only. We will further assume

$$U=-\frac{\partial \psi_0}{\partial y},$$

where $\psi_0=\psi_0(y)$ is the streamfunction in the basic state. Since U is a function of pressure only, it is seen that ψ_0 is a linear function of y for constant p. The vorticity equation, the continuity equation and the thermodynamic equation will be satisfied identically in the basic state, while the divergence equation and the hydrostatic relation reduce to

$$\left.\begin{aligned} \beta U + \frac{\partial^2 \phi_0}{\partial y^2} &= 0, \\ \frac{\partial \phi_0}{\partial p} &= -\frac{R}{p}\theta_0\left(\frac{p}{p_0}\right)^{R/Cp}. \end{aligned}\right\} \quad (2.5)$$

It is seen that ϕ_0 must be a quadratic function of y. When we integrate the first equation with respect to y and make use of the second we obtain:

$$\frac{\partial \theta_0}{\partial y} = \frac{f_0 + \beta y}{R} p^{1-\varkappa} p_0^{\varkappa} \frac{dU}{dp}, \quad (2.6)$$

where $\varkappa = R/Cp$.

One possible measure of the static stability in the atmosphere is $-\partial\theta/\partial p$. Using this measure of static stability we find the static stability in the basic state to be

$$\frac{\partial}{\partial y}\left(-\frac{\partial \theta_0}{\partial p}\right) = -\frac{f_0 + \beta y}{R}(1-\varkappa)p^{-\varkappa} p_0^{\varkappa} \frac{dU}{dp}, \quad (2.7)$$

where we have assumed that dU/dp is constant. When the expressions for the temperature and stability gradients (2.6) and (2.7) are later being used in the linerarized equation we replace $f_0 + \beta y$ by f_0.

Superimposed on the basic state as defined above we shall consider perturbations which will be assumed to be independent of the meridional direction. The perturbations will thus have the form:

$$h(x,p,t) = A(p)e^{ik(x-ct)}, \quad (2.8)$$

where h is any parameter, $A(p)$ the amplitude, k the wave number and c the wave speed.

We are next going to apply the equations to a two layer model of the atmosphere. The atmosphere is subdivided in two layers separated by the 50 cb surface. The quantities in the upper and lower layers will be measured at 25 cb and 75 cb. The boundary condition at the upper boundary will be $\omega = 0$ at $p = 0$, while the boundary condition at the lower boundary for simplicity will be $\omega = 0$ at $p_0 = 100$ cb. The levels will be numbered as indicated in Fig. 1.

Applying first the continuity equation at levels 1 and 3 we get taking finite differences:

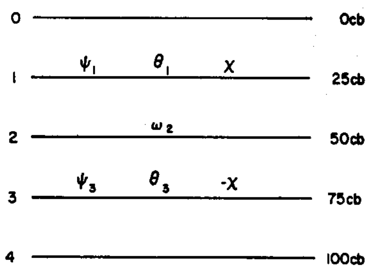

FIG. 1. The levels used in the models under investigation. The quantities entered on the figure show the places where the stream function, the velocity potential, the potential temperature and the vertical velocity are measured in the most general model, the primitive equations with horizontal variation of static stability.

$$\left.\begin{aligned} \frac{\partial^2 \chi_1}{\partial x^2} + \frac{2}{p_0}\omega_2 &= 0, \\ \frac{\partial^2 \chi_3}{\partial x^2} - \frac{2}{p_0}\omega_2 &= 0. \end{aligned}\right\} \quad (2.9)$$

Adding and subtracting the equations (2.9) we find

$$\frac{\partial^2}{\partial x^2}(\chi_1 + \chi_3) = 0; \frac{\partial^2}{\partial x^2}\left(\frac{\chi_1 - \chi_3}{2}\right) + \frac{2}{p_0}\omega_2 = 0. \quad (2.10)$$

The equations (2.10) will be satisfied if we put $\chi_1 = \chi$ and $\chi_3 = -\chi$ in which case (2.10) reduce to

$$\frac{\partial^2 \chi}{\partial x^2} + \frac{2}{p_0}\omega_2 = 0.$$

We apply next the vorticity equation in its linearized form at levels 1 and 3 and obtain:

$$\left.\begin{aligned} \frac{\partial}{\partial t}\left(\frac{\partial^2 \psi_1}{\partial x^2}\right) + U_1 \frac{\partial}{\partial x}\left(\frac{\partial^2 \psi_1}{\partial x^2}\right) + \beta \frac{\partial \psi_1}{\partial x} & \\ + f_0 \frac{\partial^2 \chi}{\partial x^2} &= 0, \\ \frac{\partial}{\partial t}\left(\frac{\partial^2 \psi_3}{\partial x^2}\right) + U_3 \frac{\partial}{\partial x}\left(\frac{\partial^2 \psi_3}{\partial x^2}\right) + \beta \frac{\partial \psi_3}{\partial x} & \\ - f_0 \frac{\partial^2 \chi}{\partial x^2} &= 0. \end{aligned}\right\} \quad (2.11)$$

Denoting

$$\psi_1 = \psi + \tau, \; \psi_3 = \psi - \tau \; U_1 = U^* + U',$$

$U_3 = U^* - U'$ we get by adding and subtracting the equations (2.11)

$$\left.\begin{aligned}\frac{\partial}{\partial t}\left(\frac{\partial^2\psi}{\partial x^2}\right) + U^*\frac{\partial}{\partial x}\left(\frac{\partial^2\psi}{\partial x^2}\right) + U'\frac{\partial}{\partial x}\left(\frac{\partial^2\tau}{\partial x^2}\right)&\\ + \beta\frac{\partial\psi}{\partial x} = 0,&\\ \frac{\partial}{\partial t}\left(\frac{\partial^2\tau}{\partial x^2}\right) + U^*\frac{\partial}{\partial x}\left(\frac{\partial^2\tau}{\partial x^2}\right) + U'\frac{\partial}{\partial x}\left(\frac{\partial^2\psi}{\partial x^2}\right)&\\ + \beta\frac{\partial\tau}{\partial x} + f_0\frac{\partial^2\chi}{\partial x^2} = 0.&\end{aligned}\right\}\quad(2.12)$$

We are next going to treat the divergence equation in a similar way. Applying this equation at levels 1 and 3 we get

$$\left.\begin{aligned}\frac{\partial}{\partial t}\left(\frac{\partial^2\chi}{\partial x^2}\right) + U_1\frac{\partial}{\partial x}\left(\frac{\partial^2\chi}{\partial x^2}\right) + \beta\frac{\partial\chi}{\partial x} + \frac{dU}{dp}\frac{\partial\omega_1}{\partial x}&\\ + \frac{\partial^2\phi_1}{\partial x^2} - f_0\frac{\partial^2\psi_1}{\partial x^2} = 0,&\\ -\frac{\partial}{\partial t}\left(\frac{\partial^2\chi}{\partial x^2}\right) - U_3\frac{\partial}{\partial x}\left(\frac{\partial^2\chi}{\partial x^2}\right) - \beta\frac{\partial\chi}{\partial x} + \frac{dU}{dp}\frac{\partial\omega_3}{\partial x}&\\ + \frac{\partial^2\phi_3}{\partial x^2} - f_0\frac{\partial^2\psi_3}{\partial x^2} = 0.&\end{aligned}\right\}\quad(2.13)$$

In adding and subtracting these equations we shall use the following relations:

$$\frac{dU}{dp} \simeq \frac{U_3 - U_1}{\frac{1}{2}p_0} = -\frac{4}{p_0}U', \qquad (2.14)$$

$$\phi^* = \tfrac{1}{2}(\phi_1 + \phi_3),\ \phi' = \tfrac{1}{2}(\phi_1 - \phi_3)$$

$$= -\tfrac{1}{2}\frac{p_0}{2}\left(\frac{\partial\phi}{\partial p}\right)_2 = \frac{R}{2^{\varkappa+1}}\theta_2. \qquad (2.15)$$

It will further be assumed that

$$\omega_1 = \omega_3 = q\omega_2, \quad q \simeq \tfrac{1}{2}. \qquad (2.16)$$

Substracting the two equations (2.13) we get:

$$\frac{\partial}{\partial t}\left(\frac{\partial^2\chi}{\partial x^2}\right) + U^*\frac{\partial}{\partial x}\left(\frac{\partial^2\chi}{\partial x^2}\right) + \beta\frac{\partial\chi}{\partial x} + \frac{R}{2^{\varkappa+1}}\frac{\partial^2\theta_2}{\partial x^2} - f_0\frac{\partial^2\tau}{\partial x^2} = 0. \qquad (2.17)$$

Adding the two equations (2.13) we get using the relations (2.14)–(2.16)

$$2U'\frac{\partial}{\partial x}\left(\frac{\partial^2\chi}{\partial x^2}\right) + \frac{\partial^2\phi^*}{\partial x^2} - f_0\frac{\partial^2\psi}{\partial x^2} = 0. \qquad (2.18)$$

The remaining two equations are obtained by applying the thermodynamic equation at levels 1 and 3. Taking vertical finite differences we get:

$$\left.\begin{aligned}\frac{\partial\theta_1}{\partial t} + \nabla\cdot(\theta_1\mathbf{v}_1) + \frac{2}{p_0}\theta_2\omega_2 = 0,\\ \frac{\partial\theta_3}{\partial t} + \nabla\cdot(\theta_3\mathbf{v}_3) - \frac{2}{p_0}\theta_2\omega_2 = 0.\end{aligned}\right\}\quad(2.19)$$

We introduce the notations $\theta_1 = \theta + \sigma, \theta_3 = \theta - \sigma$ and the approximation $\theta_2 = \theta = \frac{1}{2}(\theta_1 + \theta_3)$. When we form the sum and differences of the two equations (2.19) and linearize we get

$$\left.\begin{aligned}\frac{\partial\theta}{\partial t} + U^*\frac{\partial\theta}{\partial x} + U'\frac{\partial\sigma}{\partial x} + v\frac{\partial\theta_0}{\partial y} + v'\frac{\partial\sigma_0}{\partial y}&\\ + \sigma_0\frac{\partial^2\chi}{\partial x^2} = 0,&\\ \frac{\partial\sigma}{\partial t} + U^*\frac{\partial\sigma}{\partial x} + U'\frac{\partial\theta}{\partial x} + v\frac{\partial\sigma_0}{\partial y} + v'\frac{\partial\theta_0}{\partial y} = 0.&\end{aligned}\right\}\quad(2.20)$$

We use next the relations (2.6) and (2.7) to relate the gradients $\partial\theta_0/\partial y$ and $\partial\sigma_0/\partial y$ to the vertical wind shear U' giving:

$$\frac{\partial\theta_0}{\partial y} = -\frac{f_0}{R}2^{\varkappa+1}U' \qquad (2.21)$$

and

$$\frac{\partial\sigma_0}{\partial y} = +\frac{f_0}{R}2^{\varkappa}(1-\varkappa)U'. \qquad (2.22)$$

When these expressions are substituted in (2.19) we can finally collect the basic set of linearized equations in the following form:

$$\frac{\partial}{\partial t}\left(\frac{\partial^2\psi}{\partial x^2}\right) + U^*\frac{\partial}{\partial x}\left(\frac{\partial^2\psi}{\partial x^2}\right) + U'\frac{\partial}{\partial x}\left(\frac{\partial^2\tau}{\partial x^2}\right) + \beta\frac{\partial\psi}{\partial x} = 0,$$

$$\left.\begin{aligned}
&\frac{\partial}{\partial t}\left(\frac{\partial^2 \tau}{\partial x^2}\right) + U^* \frac{\partial}{\partial x}\left(\frac{\partial^2 \tau}{\partial x^2}\right) + U' \frac{\partial}{\partial x}\left(\frac{\partial^2 \psi}{\partial x^2}\right) \\
&\qquad\qquad + \beta \frac{\partial \tau}{\partial x} + f_0 \frac{\partial^2 \chi}{\partial x^2} = 0, \\
&\frac{\partial}{\partial t}\left(\frac{\partial^2 \chi}{\partial x^2}\right) + U^* \frac{\partial}{\partial x}\left(\frac{\partial^2 \chi}{\partial x^2}\right) + \beta \frac{\partial \chi}{\partial x} + \frac{R}{2^{\varkappa+1}} \frac{\partial^2 \theta}{\partial x^2} \\
&\qquad\qquad - f_0 \frac{\partial^2 \tau}{\partial x^2} = 0, \\
&\frac{\partial \theta}{\partial t} + U^* \frac{\partial \theta}{\partial x} + U' \frac{\partial \sigma}{\partial x} - \frac{f_0}{R} 2^{\varkappa+1} U' \frac{\partial \psi}{\partial x} \\
&\qquad\qquad + \frac{f_0}{R} 2^{\varkappa}_{(1-\varkappa)} U' \frac{\partial \tau}{\partial x} + \sigma_0 \frac{\partial^2 \chi}{\partial x^2} = 0, \\
&\frac{\partial \sigma}{\partial t} + U^* \frac{\partial \sigma}{\partial x} + U' \frac{\partial \theta}{\partial x} + \frac{f_0}{R} 2^{\varkappa}_{(1-\varkappa)} U' \frac{\partial \psi}{\partial x} \\
&\qquad\qquad - \frac{f_0}{R} 2^{\varkappa+1} U' \frac{\partial \tau}{\partial x} = 0.
\end{aligned}\right\} \quad (2.23)$$

The five equations form a closed system with the variables ψ, τ, χ, θ and σ. The first equation is the prognostic equation for the streamfunction of the mean flow, the second the prognostic equation for the streamfunction of the shear flow, the third the prognostic equation for the velocity potential at the upper (or lower) level, while the fourth and fifth equations predict the changes in the mean potential temperature and the static stability. In addition to these equations we have the diagnostic equations (2.18), (2.15) and (2.11) from which we can compute the geopotential of the mean flow, the geopotential of the shear flow and the vertical velocity at the mid-level.

The linearized equations for a number of other two-layer models frequently used in studies of the dynamics of the atmosphere can be obtained by simplifying the system (2.23).

Let us suppose that we want to find the equations for a two-layer model based upon the primitive equations, but using the assumption that the static stability is a constant. We need then only replace the last equation in (2.23) by the condition $\sigma_0 =$ constant and drop all terms in the remaining equations containing $\partial\sigma/\partial x$. If we, at the same time, use the last relation in (2.15) we get the following set of equations

$$\left.\begin{aligned}
&\frac{\partial}{\partial t}\left(\frac{\partial^2 \psi}{\partial x^2}\right) + U^* \frac{\partial}{\partial x}\left(\frac{\partial^2 \psi}{\partial x^2}\right) + U' \frac{\partial}{\partial x}\left(\frac{\partial^2 \tau}{\partial x^2}\right) \\
&\qquad\qquad + \beta \frac{\partial \psi}{\partial x} = 0, \\
&\frac{\partial}{\partial t}\left(\frac{\partial^2 \tau}{\partial x^2}\right) + U^* \frac{\partial}{\partial x}\left(\frac{\partial^2 \tau}{\partial x^2}\right) + U' \frac{\partial}{\partial x}\left(\frac{\partial^2 \psi}{\partial x^2}\right) \\
&\qquad\qquad + \beta \frac{\partial \tau}{\partial x} + f_0 \frac{\partial^2 \chi}{\partial x^2} = 0, \\
&\frac{\partial}{\partial t}\left(\frac{\partial^2 \chi}{\partial x^2}\right) + U^* \frac{\partial}{\partial x}\left(\frac{\partial^2 \chi}{\partial x^2}\right) + \beta \frac{\partial \chi}{\partial x} + \frac{\partial^2 \phi'}{\partial x^2} \\
&\qquad\qquad - f_0 \frac{\partial^2 \tau}{\partial x^2} = 0, \\
&\frac{\partial \phi'}{\partial t} + U^* \frac{\partial \phi'}{\partial x} - f_0 u' \frac{\partial \psi}{\partial x} + \frac{R\sigma_0}{2^{\varkappa+1}} \frac{\partial^2 \chi}{\partial x^2} = 0.
\end{aligned}\right\} \quad (2.24)$$

(2.24) are the linearized equations for a two-layer model based upon the primitive equations, but assuming a constant static stability. The variables are ψ, τ, χ and ϕ' (or θ). It should be remarked at this point that it has been customary to write the thermodynamic equation in the following form when used in connection with numerical prediction models:

$$\frac{\partial}{\partial t}\left(\frac{\partial \phi}{\partial p}\right) + \mathbf{v} \cdot \nabla \left(\frac{\partial \phi}{\partial p}\right) + s\omega = 0, \quad s = -\frac{\alpha}{\theta}\frac{\partial \theta}{\partial p}. \quad (2.25)$$

The linearized form of this equation corresponding to the last equation in (2.24) would be, using (2.11):

$$\frac{\partial \phi'}{\partial t} + U^* \frac{\partial \phi'}{\partial y} - f_0 U' \frac{\partial \psi}{\partial x} + \frac{p_0^2}{8} s \frac{\partial^2 \chi}{\partial x^2} = 0. \quad (2.26)$$

Complete correspondence between the two equations is therefore obtained if

$$s = \frac{8}{p_0^2} \frac{R\sigma_0}{2^{\varkappa+1}}. \quad (2.27)$$

A typical value for σ_0 corresponding to winter conditions in middle latitudes is, according to Gates (1961*a*), $\sigma_0 = 15$ deg. This value is an average value for the layer 1000–300 mb. The corresponding value of s is according to (2.27) $s = 1.4$ m^{2}sec^{-2}cb^{-2}. This value is considerably smaller than the typical values of s which are obtained from atmospheric data or from the standard atmosphere. From GATES (1961*a*) we find that the average value of s corresponding to the same conditions as above is $s = 2.6\ \mathrm{m^2 sec^{-2} cb^{-2}}$, or almost double the value found from (2.27). The value used by PHILLIPS (1954) is as large as $s = 3.6\ \mathrm{m^2 sec^{-2} cb^{-2}}$. One must pay attention to this difference when one compares the results obtained by GATES (1961*b*) and those, which will be reported in this paper. The difference noted above is naturally due to the fact that we use a two-layer representation with no vertical variation of static stability and in particular to the truncation error committed in (2.15).

The balanced two-layer models with and without horizontal variation are obtained by assuming that the divergence equation appearing in (2.23) and (2.24) is replaced by a balance equation which in the linearized version reduces to

$$\frac{R}{2^{\varkappa+1}}\frac{\partial^2\theta}{\partial x^2} - f_0\frac{\partial^2\tau}{\partial x^2} = 0, \tag{2.28}$$

or

$$\frac{\partial^2\phi'}{\partial x^2} - f_0\frac{\partial^2\tau}{\partial x^2} = 0. \tag{2.29}$$

The equations for the balanced two-layer model with horizontal variation of static stability can therefore be written:

$$\left.\begin{aligned}
&\frac{\partial}{\partial t}\left(\frac{\partial^2\psi}{\partial x^2}\right) + U^*\frac{\partial}{\partial x}\left(\frac{\partial^2\psi}{\partial x^2}\right) + U'\frac{\partial}{\partial x}\left(\frac{\partial^2\tau}{\partial x^2}\right) + \beta\frac{\partial\psi}{\partial x} = 0,\\
&\frac{\partial}{\partial t}\left(\frac{\partial^2\tau}{\partial x^2}\right) + U^*\frac{\partial}{\partial x}\left(\frac{\partial^2\tau}{\partial x^2}\right) + U'\frac{\partial}{\partial x}\left(\frac{\partial^2\psi}{\partial x^2}\right) + \beta\frac{\partial\tau}{\partial x} + f_0\frac{\partial^2\chi}{\partial x^2} = 0,\\
&\frac{R}{2^{\varkappa+1}}\frac{\partial^2\theta}{\partial x^2} - f_0\frac{\partial^2\tau}{\partial x^2} = 0,\\
&\frac{\partial\theta}{\partial t} + U^*\frac{\partial\theta}{\partial x} + U'\frac{\partial\sigma}{\partial x} - \frac{f_0}{R}2^{\varkappa+1}U'\frac{\partial\psi}{\partial x} + \frac{f_0}{R}2^{\varkappa}(1-\varkappa)U'\frac{\partial\tau}{\partial x} + \sigma_0\frac{\partial^2\chi}{\partial x^2} = 0,\\
&\frac{\partial\sigma}{\partial t} + U^*\frac{\partial\sigma}{\partial x} + U'\frac{\partial\theta}{\partial x} + \frac{f_0}{R}2^{\varkappa}(1-\varkappa)U'\frac{\partial\psi}{\partial x} - \frac{f_0}{R}2^{\varkappa+1}U'\frac{\partial\tau}{\partial x} = 0.
\end{aligned}\right\} \tag{2.30}$$

This system is identical to the one investigated by GATES (1961*b*) except for the trivial difference that we have assumed $\chi_1 = \chi$, $\chi_3 = -\chi$, while Gates has made the opposite choice.

The equations for the balanced two-layer model without horizontal variation of static stability are finally

$$\left.\begin{aligned}
&\frac{\partial}{\partial t}\left(\frac{\partial^2 x}{\partial\psi^2}\right) + U^*\frac{\partial}{\partial x}\left(\frac{\partial^2\psi}{\partial x^2}\right) + U'\frac{\partial}{\partial x}\left(\frac{\partial^2\tau}{\partial x^2}\right) + \beta\frac{\partial\psi}{\partial x} = 0,\\
&\frac{\partial}{\partial t}\left(\frac{\partial^2\tau}{\partial x^2}\right) + U^*\frac{\partial}{\partial x}\left(\frac{\partial^2\tau}{\partial x^2}\right) + U'\frac{\partial}{\partial x}\left(\frac{\partial^2\psi}{\partial x^2}\right) + \beta\frac{\partial\tau}{\partial x} + f_0\frac{\partial^2\chi}{\partial x^2} = 0,\\
&\frac{\partial^2\phi'}{\partial x^2} - f_0\frac{\partial^2\tau}{\partial x^2} = 0,\\
&\frac{\partial\phi'}{\partial t} + U^*\frac{\partial\phi'}{\partial x} - f_0U'\frac{\partial\psi}{\partial x} + \frac{R\sigma_0}{2^{\varkappa+1}}\frac{\partial^2\chi}{\partial x^2} = 0.
\end{aligned}\right\} \tag{2.31}$$

The remarks made earlier about the numerical values of the stability parameter s and $R\sigma_0 2^{-\varkappa-1}$ apply naturally again in any comparison of (2.30) and (2.31).

It should furthermore be remarked that the balance equation for the mean flow (2.18) in the linearized versions of the balanced model is replaced by

$$\frac{\partial^2\phi^*}{\partial x^2} - f_0\frac{\partial^2\psi}{\partial x^2} = 0. \tag{2.32}$$

3. Primitive and balanced models with constant static stability

In this section we are going to compare solutions to the linearized equations for the two layer models when the static stability is assumed constant. The linearized equations were derived in Section 2 (system (2.24) and (2.31)).

When we substitute expressions of the type (2.8) in (2.24) we get a set of linear homogeneous equations in the (complex) amplitudes. Denoting the disturbances by $\psi = \hat{\psi} e^{ik(x-ct)}$ and analogous expressions for the other variables we find the following set of linear homogeneous equations

$$\left.\begin{aligned} &\xi\hat{\psi} + U\hat{\tau} = 0, \\ &U'\hat{\psi} + \xi\hat{\tau} - ik\frac{f_0}{k^2}\hat{\chi} = 0, \\ &ik\frac{f_0}{k^2}\hat{\tau} + \xi\hat{\chi} - ik\frac{1}{k^2}\hat{\phi}' = 0, \\ &-f_0 U'\hat{\psi} + ik\frac{R\sigma_0}{2^{\varkappa+1}}\hat{\chi} + \left(\xi + \frac{\beta}{k^2}\right)\hat{\phi}' = 0, \end{aligned}\right\} \quad (3.1)$$

where

$$\xi = U^* - c - \beta/k^2. \quad (3.2)$$

These equations will have non-zero solutions if the determinant vanishes. This condition leads to the following fourth degree equation in ξ:

$$\xi^4 + \frac{\beta}{k^2}\xi^3 - \left(U'^2 + \frac{f_0^2}{k^2} + \frac{R\sigma_0}{2^{\varkappa+1}}\right)\xi^2 - \frac{\beta}{k^2}\left(U'^2 + \frac{f_0^2}{k^2}\right)\xi + \left(\frac{R\sigma_0}{2^{\varkappa+1}} - \frac{f_0^2}{k^2}\right)U'^2 = 0. \quad (3.3)$$

Equations of this type will result for the four different models which we compare in this study. In each case, except the one leading to a quadratic equation, the equation has been solved on an electronic computer. The values of β, f_0, and σ_0 were kept at constant values during each calculation, while U' and the wave-length $L = 2\pi/k$ varied. For the particular equation (3.3) L varied between 1000 and 28,000 km in increments of 1000 km, while the vertical wind shear dU/dz measured in $\mathrm{m\,sec^{-1}km^{-1}}$ varied between 0.5 and 15 m $\mathrm{sec^{-1}km^{-1}}$ in increments of 0.5 m $\mathrm{sec^{-1}km^{-1}}$. The value of U' in $\mathrm{m\,sec^{-1}}$ is related to dU/dz in $\mathrm{m\,sec^{-1}km^{-1}}$ through the approximate formula.

$$U' \simeq 5\frac{dU}{dz}. \quad (3.4)$$

It is easily seen that the only thing which happens when the system (2.31) is treated in the same way as (2.24) is that the term containing ξ as coefficient in the third equation disappears. This term refers to the local and advective changes of divergence and the β-term in the divergence equation. The equation corresponding to (3.3) reduces to a second degree equation in ξ which may be written:

$$\left(\frac{f_0^2}{k^2} + \frac{R\sigma_0}{2^{\varkappa+1}}\right)\xi^2 + \frac{\beta}{h^2}\frac{f_0^2}{k^2}\xi + \left(\frac{f_0^2}{k^2} - \frac{R\sigma_0}{2^{\varkappa+1}}\right)U'^2 = 0. \quad (3.5)$$

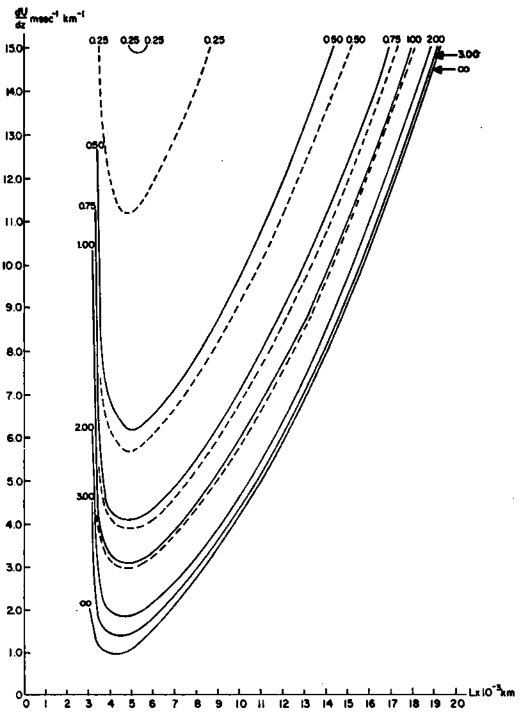

FIG. 2. Stability diagram for the models with constant static stability. The abscissae is the wavelength measured in thousands of kilometers and the ordinate the vertical windshear in $\mathrm{msec^{-1}km^{-1}}$. The solid curves are the e-folding times in days for the primitive equations, while the dashed curves give the same quantity for the balanced model. ($\beta = 16 \times 10^{-12}\mathrm{m^{-1}sec^{-1}}$, $f_0 = 10^{-4}\mathrm{sec^{-1}}$, $\sigma_0 = 21$ deg.)

The solutions of (3.3) and (3.5) may be compared to find the differences in the speed of propagation and amplification rate of the wave-solutions to the primitive equations and the filtered equations in the case of constant static stability.

Fig. 2 contains curves describing the e-folding time of unstable disturbances computed from the primitive equations (solid curves) and the filtered equations (dashed curves). This diagram was computed for the following values of the parameters $\beta = 16 \times 10^{-12} \mathrm{m}^{-1} \mathrm{sec}^{-1}$, $f_0 = 10^{-4} \mathrm{sec}^{-1}$ and $\sigma_0 = 21$ deg. The last value of σ_0 corresponds to a value of $s = 2$ m^{2}sec^{-2}cb^{-2}. It is seen from Fig. 2 that there is very little difference between the amplification rate computed from the primitive equations and the filtered equations. As a matter of fact, it is impossible to separate the two families of curves on the diagram when we are in the neighborhood of the curve for neutral stability. Within the observed values of dU/dz it is found that only small differences occur. Only in the case where dU/dz is very large do we get significant differences between the two sets of curves. This result could, as a matter of fact, be expected, because it is known (EADY, 1949; GREEN, 1960) that the assumption of balance or geostrophy breaks down when the Richardson number becomes small.

The Richardson number is usually defined as

$$Ri = g \frac{d \ln \theta}{dz} \Big/ \left(\frac{dU}{dz}\right)^2. \tag{3.6}$$

It is easily seen, using the hydrostatic equation, that the Richardson number may also be expressed

$$Ri = s \Big/ \left(\frac{dU}{dp}\right)^2, \tag{3.7}$$

where s is defined in (2.25).

In terms of our variable U' we find

$$Ri = \frac{p_0^2}{16} \frac{s}{U'^2}. \tag{3.8}$$

A typical value of U' for summer conditions is 10 msec^{-1}, in which case $Ri = 12$ for $s = 2$, while $U' = 20$ msec^{-1} corresponds to typical winter conditions giving a value of $Ri = 3$. We find differences in the amplification rate of about 6% at $dU/dz = 6$ msec^{-1}km^{-1}, and $L =$ 5000 km, which corresponds to a Richardson number of 1.4. For $dU/dz = 10$ msec^{-1}km^{-1} and $L = 5000$ km the difference in amplification rate between the two models is 15% and $Ri = \frac{1}{2}$, while $dU/dz = 7$ msec^{-1}km^{-1} and $L = 5000$ km gives a difference of 9% and $Ri = 1$. As a result of these examples we find that if the Richardson number is about 1 we find differences between the amplification rates computed from the primitive equations and the balanced equations of about 10%. However, this result should only be taken as an example simply because we have only used a single static stability.

The discussion above summarizes the comparison between the amplification rate in the linear primitive equation model and the linear balanced model in the case where the static stability has no horizontal variation. It is interesting to compare also the speed of propagation of the waves in the same case. It will be noted from the solution of equation (3.5), which applies to the filtered model, that the speed of propagation of the *unstable* waves is independent of the vertical wind shear. The difference between the speed of propagation in the two models is therefore conveniently investigated in diagrams where the speed of propagation is plotted as a function of vertical wind shear for different values of the horizontal wave length. Fig. 3 shows such a comparison for $L = 5000$ km. The vertical line in this figure is the speed of propagation of the unstable wave in the balanced model, while the other curve shows the same quantity in the primitive model. It is seen that there is a good agreement between the two curves for small values of the vertical wind shear, while the difference becomes larger for increasing values of dU/dz. For the largest value of dU/dz included in the calculations ($dU/dz = 15$ msec^{-1}km^{-1}) we find a difference of about 8%, but it should be mentioned that this value of the vertical wind shear is several times larger than the value normally observed in the atmosphere even in the winter season. Fig. 4 shows a similar comparison for $L =$ 10,000 km. Qualitatively the result is the same. The agreement is best for small values of the wind shear. It is noted that the speed of propagation is numerically larger, in both cases, in the primitive model than in the balanced model.

We are next going to investigate the structure of the unstable baroclinic wave in the two models. This can be done by going back to the system (3.1). When the solution to the frequency equation (3.3) (or (3.5) in the balanced model) is known, we know the values of the coefficients in (3.1). By assuming the numerical value of one of the unknowns in (3.1) we may solve for the values of the remaining amplitudes. The result of such a calculation is summarized in Fig. 5 for the primitive model. It was assumed

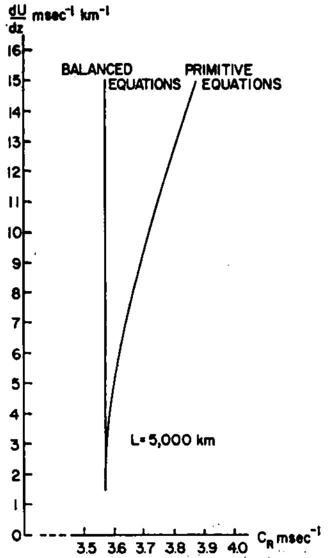

FIG. 3. The speed of propagation of unstable disturbances, measured in msec^{-1}, as a function of the vertical windshear in $\mathrm{msec}^{-1}\mathrm{km}^{-1}$ for $L = 5000$ km. The vertical line is for the balanced model, while the other curve is for the primitive equations.

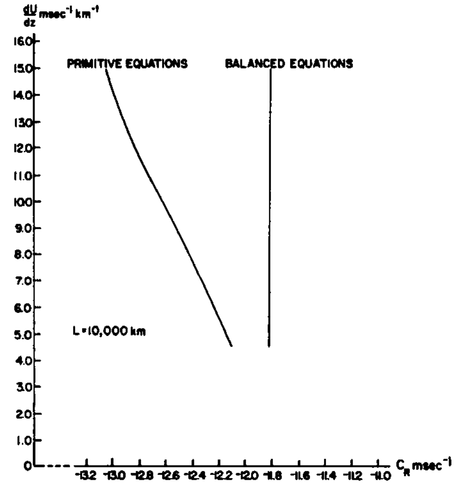

FIG. 4. As Fig. 3, except $L = 10{,}000$ km.

in this calculation that the wave length was $L = 5000$ km, the vertical wind shear $dU/dz = 4$ m $\mathrm{sec}^{-1}\mathrm{km}^{-1}$ and the static stability parameter $s = 2\ \mathrm{m}^2\mathrm{sec}^{-2}\mathrm{cb}^{-2}$. It was further assumed that the meridional mean wind, derived from ψ in (3.1) was

$$v^* = \partial\psi/\partial x = \hat{v}^* \cos kx, \tag{3.9}$$

where $\hat{v}^* = 10\ \mathrm{msec}^{-1}$.

The two upper curves in Fig. 5 (a and b) show the variation of the meridional wind components, v_1 and v_3, at the two levels. It is seen that the unstable baroclinic wave has the usual slope toward the west with decreasing pressure. The amplitude of the meridional wind is somewhat larger at the upper level. The two middle curves in Fig. 5 (c and d) show the geopotential as a function of x for the upper and lower level. If the flow were strictly geostrophic these curves would be displaced 90° to the right in the figure relative to the curves showing the meridional winds. Any difference in the phase from the 90° displacement and of course differences in the proper amplitude show the presence of ageostrophic wind components. The distribution of the ageostrophic wind can be

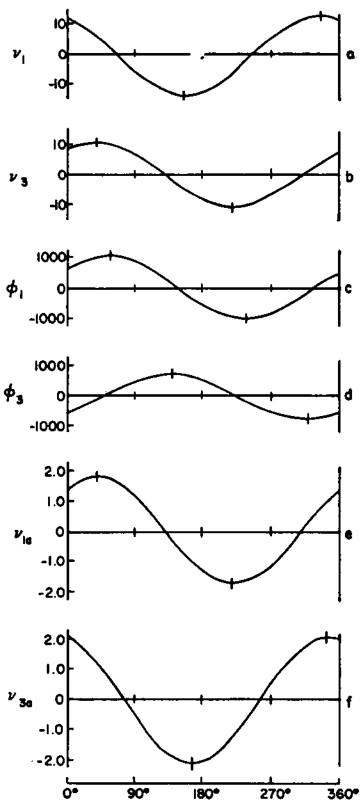

FIG. 5. The distribution over one wavelength of meridional wind velocities, geopotentials and ageostrophic, meridional wind velocities at the upper and lower levels for an unstable baroclinic wave, computed from the primitive equations with constant static stability. ($L = 5000$ km, $dU/dz = 4$ m $\mathrm{sec}^{-1}\mathrm{km}^{-1}$, otherwise parameters as in Fig. 2.)

TABLE 1.

Parameter	Amplitude	Position of ridge	Amplitude	Position of ridge
v_1	13.31	-27.5	13.40	-28.3
v_3	10.24	$+36.8$	10.36	$+38.8$
ψ_1	10.60×10^6	$+62.5$	10.67×10^6	$+61.7$
ψ_3	8.15×10^6	$+126.8$	8.25×10^6	$+128.8$
ϕ_1	1014	$+55.2$	1067	$+61.7$
ϕ_3	724	$+137.7$	825	$+128.8$
v_{1a}	1.75	$+39.5$	—	—
v_{3a}	2.10	-15.4	—	—
ω_2	2.17×10^{-4}	-170.7	2.21×10^{-4}	-170.6
	Primitive equations		Balanced equations	

found by computing the geostrophic wind from the distribution of ϕ_1 and ϕ_3 and next subtract the geostrophic wind from the total wind. The result of the calculation is shown in the curves e and f at the bottom of Fig. 5. The scale of the curves for the ageostrophic wind has been increased 10 times relative to the scale for the total wind. The distribution of the ageostrophic wind at the upper level is such that the wind is supergeostrophic around the ridge in the geopotential with a maximum close to the maximum geopotential and subgeostrophic around the trough in the geopotential. A comparison between the geopotential and the ageostrophic wind at the lower level shows by and large the opposite arrangement with supergeostrophic winds around the ridge in the geopotential.

A figure similar to Fig. 5 can naturally be prepared for the balanced model, but in this model there is, by definition, no ageostrophic wind. The difference between the other components is so small that one can hardly see the difference on a figure. We have therefore preferred to summarize the results in Table 1.

It is seen from Table 1 that when we start out by assuming the same distribution of the mean meridional wind we find only small differences in v_1 and v_3 (and naturally also in ψ_1 and ψ_3). The greatest difference must show up in the geopotential simply because the geopotential is computed directly from the wind through the geostrophic assumption in the balanced model, while this is not the case in the primitive equations. The difference in the geopotential amounts to about 5% at the upper level in our example and to about 14% at the lower level. These figures are consistent with the fact that the ageostrophic wind is somewhat larger at the lower level combined with the fact that the amplitudes are smaller at this level. We notice, furthermore, by comparing the phase-angles for ϕ_1 and ϕ_3 in the two models that the slope in this quantity is 67.1 degrees in the balanced model, but 82.5 degrees in the primitive models. In this connection it should be noticed that 360 degrees corresponds to a full-wave-length. The slope between the two levels, which are 50 cb apart, corresponds in other words to 19 and 23% of the wave-length, respectively. We finally notice that there is only a very small difference in the amplitude and phase of the vertical velocity.

In summary, we find that the main difference between the two models is the presence of the ageostrophic wind in the primitive equations. This difference can be summarized as follows: At the upper level the wind is supergeostrophic in the ridge and subgeostrophic in the trough. The amplitude of the ageostrophic winds is 13% of the amplitude of the total wind at the upper level. The wind is supergeostrophic at the lower level in the trough, but subgeostrophic in the ridge. The amplitude of the ageostrophic wind is 20% of the amplitude of the total wind at this level.

4. Primitive and balanced models with variable static stability

The comparison which was performed in the preceding section of the primitive and balanced equations in the case of constant static stability can naturally be extended to the case of variable static stability. This will be done in this section. The basic equations for the models which are to be compared are summarized in the systems (2.23) and (2.30), of which (2.30) as mentioned before, is identical to the model investigated by GATES (1961*b*).

Using perturbations of identically the same form as before we find the following set of linear homogeneous equations corresponding to the system (3.1):

$$\left.\begin{aligned}
&\xi\hat{\psi} + U'\hat{\tau} = 0,\\
&U'\hat{\psi} + \xi\hat{\tau} - ik\frac{f_0}{k^2}\hat{\chi} = 0,\\
&-\frac{f_0}{R}2^{\varkappa+1}U'\hat{\psi} + \frac{f_0}{R}2^{k}(1-\varkappa)U'\hat{\tau} + \left(\xi + \frac{\beta}{h^2}\right)\hat{\theta}\\
&\qquad + U'\hat{\sigma} + ik\sigma_0\hat{\chi} = 0,\\
&+\frac{f_0}{R}2^{k}(1-\varkappa)U'\hat{\psi} - \frac{f_0}{R}2^{\varkappa+1}U'\hat{\tau} + U'\hat{\theta}\\
&\qquad + \left(\xi + \frac{\beta}{k^2}\right)\hat{\theta} = 0,\\
&-ik\frac{f_0}{k^2}\hat{\tau} + \frac{R}{2^{\varkappa+1}}\frac{ik}{k^2}\hat{\theta} - \xi\hat{\chi} - 0.
\end{aligned}\right\} \tag{4.1}$$

The symbols used here are the same as before, and the quantity ξ is defined by (3.2). The equation for the determination of ξ which is obtained by setting the determinant of the system (4.1) equal to zero turns out to be the following fifth degree equation:

$$\begin{aligned}
&\xi^5 + 2\frac{\beta}{k^2}\xi^4 - \left(2U'^2 + \frac{f_0^2}{k^2} + \frac{R\sigma_0}{2^{\varkappa+1}} - \left(\frac{\beta}{k^2}\right)^2\right)\xi^3\\
&- \left(\frac{R\sigma_0}{2^{\varkappa+1}}\frac{\beta}{k^2} + 2\frac{\beta}{k^2}\frac{f_0^2}{k^2} + \frac{1-\varkappa}{2}\frac{f_0^2}{k^2}U' + 2\frac{\beta}{k^2}U'^2\right)\xi^2\\
&- \left(\frac{f_0^2}{k^2}\left(\frac{\beta}{k^2}\right)^2 + \frac{1-\varkappa}{2}U'\frac{f_0^2}{k^2}\frac{\beta}{k^2} + \left(\frac{\beta}{k^2}\right)^2U'^2\right.\\
&\left. - \frac{R\sigma_0}{2^{\varkappa+1}}U'^2 - U'^4 + \frac{f_0^2}{k^2}U'^2\right)\xi\\
&+ \left(\frac{R\sigma_0}{2^{\varkappa+1}}U'^2\frac{\beta}{k^2} - \frac{1-\varkappa}{2}\frac{f_0^2}{k^2}U'^3 - \frac{f_0^2}{k^2}U'^2\frac{\beta}{k^2}\right) = 0.
\end{aligned} \tag{4.2}$$

The values of the parameters which were used in the solution of (4.2) were $\beta = 16 \times 10^{-12}$ $m^{-1}sec^{-1}$, $f_0 = 10^{-4}sec^{-1}$, and $\sigma_0 = 15$ deg. The last value was selected to coincide with one of the values used by GATES (1961*b*) in his study. The values of L and dU/dz varied in the same way as in the preceding section.

The equation for the wave-speed in the case of a balanced two-level model with variable static stability is found by putting the determinant to zero in a set of linear homogeneous equations obtained from (4.1) by neglecting the last term in the last equation. This frequency equation turns out to be

$$\begin{aligned}
&\left(\frac{R\sigma_0}{2^{\varkappa+1}} + \frac{f_0^2}{k^2}\right)\xi^3 + \left(\frac{R\sigma_0}{2^{\varkappa+1}}\frac{\beta}{k^2} + 2\frac{\beta}{k^2}\frac{f_0^2}{k^2} + \frac{1-\varkappa}{2}U'\frac{f_0^2}{k^2}\right)\xi^2\\
&+ \left(\frac{f_0^2}{k^2}\left(\frac{\beta}{k^2}\right)^2 + \frac{1-\varkappa}{2}U'\frac{\beta}{k^2}\frac{f_0^2}{k^2} - U'^2\frac{R\sigma_0}{2^{\varkappa+1}} + \frac{f_0^2}{k^2}U'^2\right)\xi\\
&+ \left(\frac{1-\varkappa}{2}U'^3\frac{f_0^2}{k^2} + U'^2\frac{f_0^2}{k^2}\frac{\beta}{k^2} - U'^2\frac{R\sigma_0}{2^{\varkappa+1}}\frac{\beta}{k^2}\right) = 0.
\end{aligned} \tag{4.3}$$

This equation is identical to the equation investigated by GATES (1961*b*).

The two frequency equations (4.2) and (4.3) were solved by numerical methods in the same way as the equations for the models with constant static stability. The diagram giving the *e*-folding time measured in days is given in Fig. 6. The abscissa is the wave-length measured in thousands of kilometers, while the ordinate is the vertical wind shear in the unit: $m\,sec^{-1}$ km^{-1}. The figure gives only the amplification rate for $L \leqslant 10{,}000$ km. In the interval treated here there exists only one set of complex roots. It is the amplification rate corresponding to the complex root with a positive imaginary part which is given in Fig. 6. The solutions to (4.3) with the values of the parameters given above is therefore identical to GATES (1961*b*). We verify Gates' results that the wavelength of maximum instability is shifted towards shorter waves. The same is true for the cut-off wavelength below which all waves are stable. This is essentially due to the somewhat smaller value of σ_0 used in these calculations compared to the value used in the models with constant static stability. The two values of σ_0 are $\sigma_0 = 21$ degrees for the model with constant static stability and $\sigma_0 = 15$ degrees for the other model.

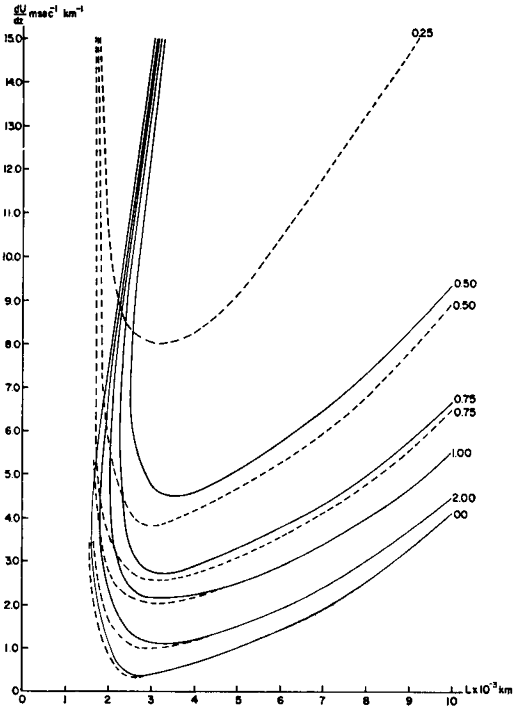

FIG. 6. Stability diagram for the models with variable static stability. Coordinates as in fig. 2. The solid curves are the e-folding times in days for the primitive equations, while the dashed curves correspond to the balanced model. ($\beta = 16 \times 10^{-12} \mathrm{m}^{-1}\mathrm{sec}^{-1}$, $\sigma_0 = 15$ deg.)

We notice the following differences between the balanced and primitive equation models: the balanced model has a cut-off wavelength around 1600 km, while the calculations based upon the primitive equations show that the lines for equal e-folding time bends towards higher wavelengths as the vertical wind shear increases. This means that waves with a given wavelength only are unstable in a certain interval of the vertical wind shear. As an example we find that waves with a wavelength of 2000 km are unstable between $dU/dz \simeq 1$ m sec^{-1}km^{-1} and $dU/dz \simeq 7.5$ m sec^{-1}km^{-1}. It is further noticed that there are only small differences between the amplification rate in the two models for small values of the wind shear, but that the difference increases for increasing values of the vertical wind shear. The difference is always such that the balanced model is more unstable. This agrees with the differences we have found in the comparison of the two models with constant static stability. However, in the present case we find differences which are considerably larger. For $dU/dz = 4$ m sec^{-1}km^{-1} which is an average wind shear in middle latitudes in winter, the differences may be as large as 30 % in the e-folding time.

We are next going to investigate the structure of the unstable baroclinic wave. For this purpose we use the equations (4.1) to find the distribution of the parameters once we have assumed the distribution for one of them. As in the previous examples we assume the distribution of the average meridional wind, see (3.9). The two upper curves in Fig. 7 (a and b) show the distribution of the meridional wind-components at the upper and lower level. The amplitude is slightly larger at the upper level, but the main difference is the usual westward tilt of the unstable baroclinic wave. The tilt is about $\frac{1}{8}$ of a wave-length in the meridional wind-components. The next two curves (c and d) show the distribution of the geopotential at the two levels. We find again a slightly larger amplitude at the upper level and the westward tilt. Notice that the tilt is considerably larger in the geopotential than it is in the wind-components, which shows that ageostrophic wind components are present. These components are graphed as curves e and f in Fig. 7. We find a distribution of the ageostrophic winds which is very similar to the distributions in the primitive equation model investigated in the previous section. Especially important is the fact that the maximum ageostrophic wind occurs close to the ridge at the upper level, but close to the trough at the lower level. The amplitude of the ageostrophic wind is a little larger at the lower level than at the upper. By and large we find that the ageostrophic wind is about 20 % of the total meridional wind.

In the present model we can find the distribution of temperature in the baroclinic wave at the two levels. These distributions are given in curves g and h in Fig. 7. We find that the two temperature curves are almost, but not quite in phase, but that the amplitude is about four times greater at the lower level. Fig. 7i gives finally the distribution of $\omega \times 10^4$cb sec^{-1} through the wave. It will be seen that $(-\omega)$ is almost in phase with the temperature distributions at the two levels giving a positive conversion from eddy potential to eddy kinetic energy.

In the models presently under investigation

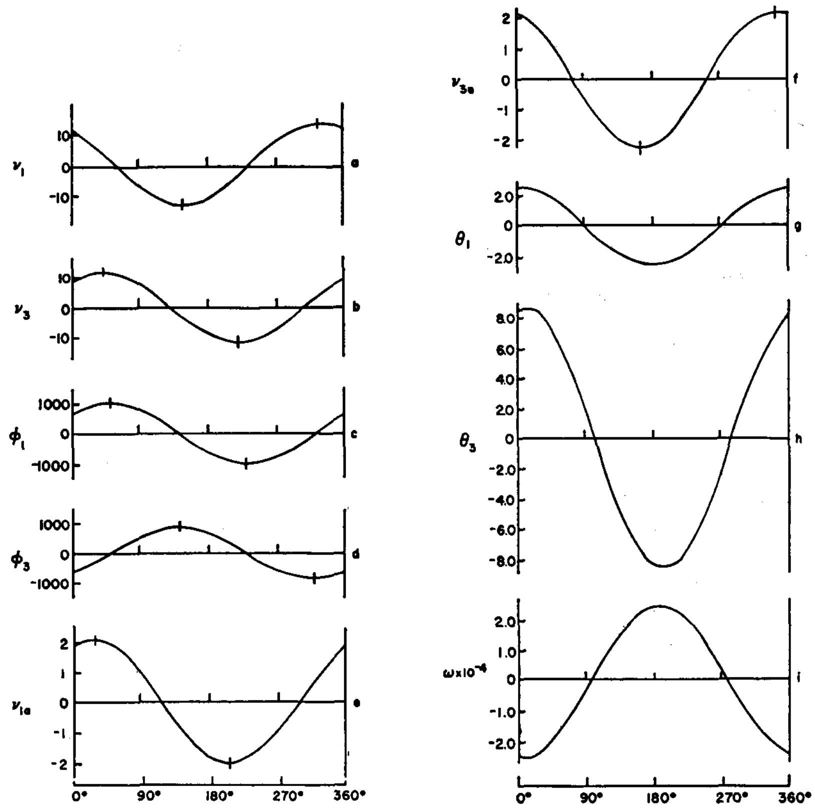

FIG. 7. The distribution over one wavelength of meridional wind velocities, geopotentials, ageostrophic meridional wind velocities, potential temperatures and vertical velocity for an unstable baroclinic wave, computed from the primitive equations with variable static stability. ($L = 5000$ km, $dU/dz = 4$ msec^{-1}, otherwise parameters as in Fig. 6.)

we have a possibility to investigate the distribution of the static stability in the perturbations. This quantity can be measured directly by the difference in potential temperature at the levels 1 and 3, but we shall prefer to use one of the measures of static stability investigated from observations by GATES (1961*a*). Most of his distributions are given using the following measure

$$s^* = -\frac{T}{\theta}\frac{\partial\theta}{\partial p}. \tag{4.4}$$

Using finite differences we get:

$$s^* = \frac{4}{p_0} 2^{\varkappa}\sigma, \tag{4.5}$$

where σ as before is defined as

$$\sigma = \tfrac{1}{2}(\theta_1 - \theta_3). \tag{4.6}$$

Substituting the numerical values we get

$$\sigma = 3.04 s^*, \tag{4.7}$$

where s^* now is measured in the unit: deg db^{-1}, the unit used by GATES (loc. cit.). The averaged value of s^* for the layer 250–750 mb is approximately 5 deg db^{-1}, which justifies the choice of $\sigma_0 = 15$ degrees used in our calculations for the stability in the basic state.

Using the values of θ_1 and θ_3 we find the distribution of s^* in the unstable baroclinic wave. This distribution is given in Fig. 8 together with the distribution of the geopotential at the midlevel. By and large we can say that the static stability is modified in such a way that the stratification becomes more stable be-

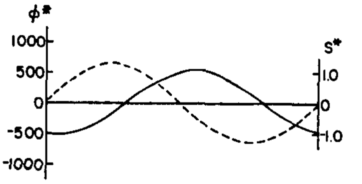

FIG. 8. The solid curve is the distribution of static stability over one wavelength in an unstable baroclinic wave in a balanced model with variable static stability, while the dashed curve is the geopotential at the mid-level. Parameters as in Figs. 6 and 7. A similar distribution is found for the primitive equations with variable static stability.

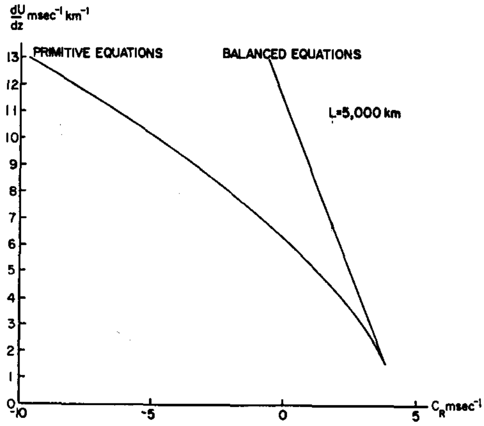

FIG. 9. The speed of propagation of unstable disturbances, measured in msec^{-1}, as a function of the vertical windshear in msec^{-1}km^{-1} for $L = 5000$ km. The two curves correspond to the balanced and primitive equations as indicated.

tween the ridge and trough, but less stable between the trough and the ridge looking downstream. The amplitude in the perturbation stability is about 20% of the stability s^* in the basic state. The author is not aware of any investigation in which a measure of the static stability has been systematically mapped relative to developing baroclinic disturbances, but it should be possible to verify the prediction of this characteristic distribution by selecting a few cases of growing baroclinic waves. The horizontal distributions of s^* given by GATES (1961*a*) has not been in any way related to the geopotential field and cannot, therefore, be used to investigate the prediction. In addition, the distributions are averaged over very long periods in time.

The comparison between the models based upon the primitive equations and the balanced equations can be made from Table 2. This table shows that the amplitudes of the ageostrophic winds are about 15–20% of the amplitudes of the total meridional wind, that the amplitudes of the meridional winds, the geopotentials and the potential temperatures are somewhat larger in the model based upon the balanced equations than they are in the primitive equation model and that the slope of the disturbance in the geopotential is somewhat larger in the primitive equation model, while the slope of the temperature disturbance is larger in the balanced model.

We shall finally investigate the speed of pro-

TABLE 2.

Parameter	Amplitude	Position of ridge	Amplitude	Position of ridge
v_1	13.38	−33.7	13.98	−34.7
v_3	11.56	+39.9	11.66	+43.1
ψ_1	10.65×10^6	+56.3	11.13×10^6	+55.3
ψ_3	9.20×10^6	+129.9	9.28×10^6	+133.1
ϕ_1	998.4	+48.0	1113.0	555.3
ϕ_3	828.9	+140.2	928.0	133.1
v_{1a}	2.05	+28.3	—	—
v_{3a}	2.27	−14.9	—	—
ω_2	2.48×10^{-4}	−173.8	2.58×10^{-4}	−171.8
θ_1	2.56	+0.3	2.76	−3.0
θ_3	8.64	+11.8	8.14	+15.2
s^*	1.01	−163.4	0.92	−155.9
ϕ^*	636.5	88.6	796.3	90
	Primitive equations		Balanced equations	

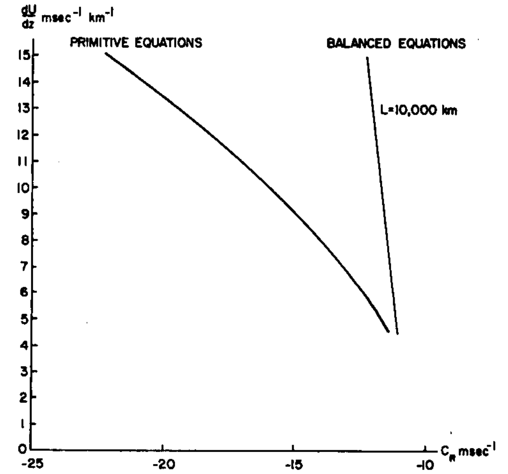

FIG 10. As Fig. 9 with $L = 10{,}000$ km.

pagation of the baroclinically unstable wave in the models with variable static stability. In Fig. 9 we have plotted the speed of propagation c_R as a function of the vertical wind shear for a fixed value of the horizontal wave length. Fig. 9 corresponds to $L = 5000$ km. We find that c_R decreases almost linearly with increasing values of the vertical wind shear in the model based upon the balanced equations, while c_R decreases more than linearly in the model based upon the primitive equations. The difference between the two speeds is very small for small values of the wind shear, but amounts to several meters per sec for large values of dU/dz. For $dU/dz = 10$ msec^{-1}km^{-1} we find a difference of approximately 5 msec^{-1}, which corresponds to a difference of more than 400 km per day. Fig. 10 contains the same information for $L =$ 10,000 km. It is seen that the difference in c_R between the models based upon the balanced and primitive equations is much larger in the case of variable static stability than it is in the case of constant stability. No other direct comparison is possible between Figs. 9 and 10 and Figs. 3 and 4, respectively, simply because the computations are based upon different values of the static stability in the basic state.

5. Very long waves

The solutions of the frequency equations for the four models were in all cases extended to include solutions corresponding to very long waves. It is well known that the two parameter, quasi-geostrophic model with constant static stability only gives stable solutions when the wave length is very large, and the vertical wind shear has values corresponding to observed values in the atmosphere. The same result was found for the balanced model with variable static stability and the primitive model with constant static stability. However, for the last model based on the primitive equations and with variable static stability it turns out that the very long waves are unstable. The curves giving the e-folding time measured in days are shown in Fig. 11 in a diagram with the wave length as abscissa and the vertical wind shear as ordinate. Fig. 11 is an extension of Fig. 6 to larger wave lengths.

The upper left part of Fig. 11 is the continuation of the region of instability shown in Fig. 6. The region to the right in Fig. 11 is the new region of instability. The curves show that the amplification rate in this region is much smaller than the one we found for smaller wavelengths. For values of the vertical wind shear characteristic of the atmosphere we find e-folding times of the order of 3–5 days for $L = 28{,}000$ km (corresponding to wave-number 1) while the e-folding time is of the order of a week for $L =$ 14,000 km.

Two important questions arise due to this result: is this result due to the simple linear formulation on the beta plane, which has been used in this study? If not, one should expect to find a weak instability also when the non-linear, primitive equations for the model with variable static is integrated numerically without any restrictions on the variation of the Coriolis parameter in the non-viscous and adiabatic case. A conclusive answer to this question can probably only be given by performing a numerical experiment where the calculation described above is carried out, because it is very difficult, if not impossible, to justify the beta plane approximation for the very long waves under consideration in this section.

The next question is: if an instability is present in the model in the non-linear formulation for very long waves, will this instability also be present in the atmosphere? In the case of the usual baroclinic instability, with a maximum amplification rate around 4000–6000 km, we find at least a qualitative agreement between

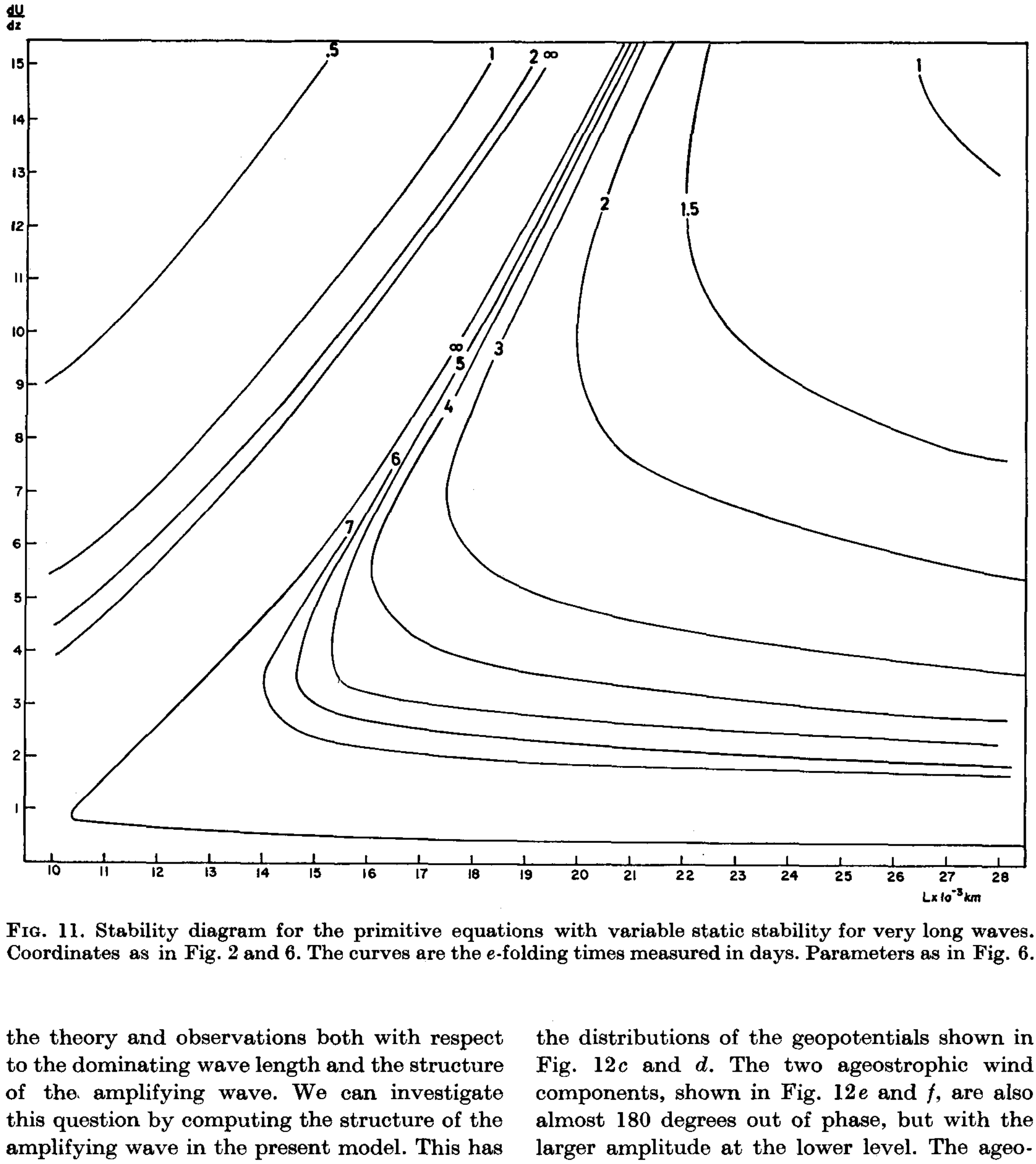

FIG. 11. Stability diagram for the primitive equations with variable static stability for very long waves. Coordinates as in Fig. 2 and 6. The curves are the e-folding times measured in days. Parameters as in Fig. 6.

the theory and observations both with respect to the dominating wave length and the structure of the amplifying wave. We can investigate this question by computing the structure of the amplifying wave in the present model. This has been done in a manner similar to the procedure which was followed in Section 4. The result of this calculation is summarized in Fig. 12*a*–*i*. In the calculations we have assumed that the meridional mean wind $v^* = \frac{1}{2}(v_1 + v_3)$ has the amplitude 1 $\mathrm{m\,sec^{-1}}$ and the maximum value at 0 degree. We see from Fig. 12*a* and *b* that the meridional wind components at the two levels are almost 180 degrees, out of phase. The larger amplitude occurs at the upper level. Exactly the same statements can be made with respect to the distributions of the geopotentials shown in Fig. 12*c* and *d*. The two ageostrophic wind components, shown in Fig. 12*e* and *f*, are also almost 180 degrees out of phase, but with the larger amplitude at the lower level. The ageostrophic components are almost in phase with the total meridional wind components which means that maximum ageostrophic wind components occur almost at the inflection point between the trough and the ridge in the geopotential, looking downstream. At the upper level we find that the ageostrophic wind is a few per cent of the total wind, while the corresponding number at the lower level is 20%. Fig. 12*g* and *h* gives the distribution of the potential temperature at the two levels. We

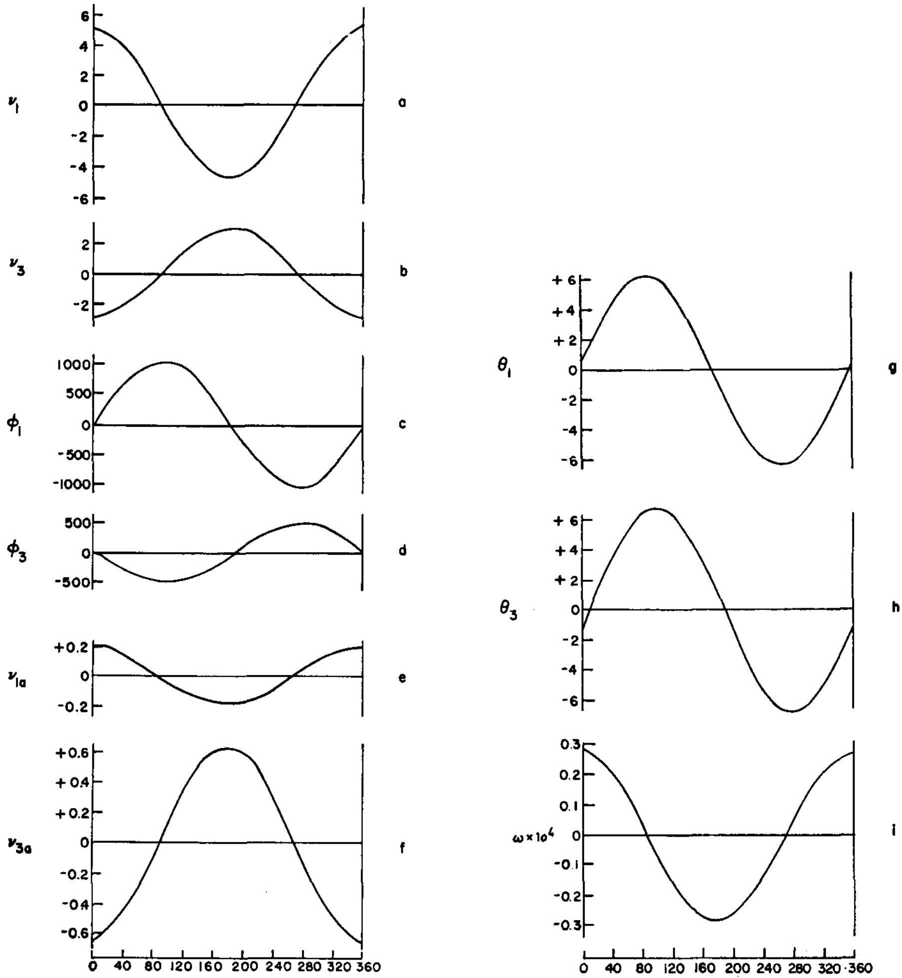

FIG. 12. The distribution over one wavelength of meridional wind velocities, geopotentials, ageostrophic meridional wind velocities, potential temperatures and vertical velocity for an unstable baroclinic wave, computed from the primitive equations with variable static stability ($L - 14{,}000$ km, $dU/dz = 4$ msec^{-1}km^{-1}, otherwise parameters as in Fig. 6).

find in this case a very small phase-difference and almost the same amplitude, which means that only a small variation exists in the static stability through the wave. The vertical velocity at the mid level is finally shown in Fig. 12*i*.

The distributions shown in Fig. 12 should be compared with the observed structure of the very long waves in the atmosphere. The observed slope of the geopotential of wave-numbers 1, 2 and 3 is shown in WIIN-NIELSEN (1961*b*) for the normal maps for January. It turns out that the observed sloped is considerably smaller than the slope which we have found in our model. This means that even if the instability of the very long waves is present in the non-linear form of the primitive equations in a model with variable static stability, there is no close correspondence between these waves and the very long waves observed in the atmosphere. This result is not too surprising because it has been shown (WIIN-NIELSEN, 1961*a*) that the phase-difference between the temperature and geopotential fields, which is closely related to the vertical slope of the waves, is rather sensitive to the surface skin function in the case of stationary waves. One might therefore expect to find some change in the vertical structure of the waves also in this case if friction were included. The result of such a study will be reported later.

Our main conclusion is therefore that the weak instability which we have found for very long waves in a model based upon the primitive equations and with a variable static stability, will result in waves with a structure rather different from the observed structure of very long waves in the atmosphere. This difference can possibly be due to the fact that friction was not included in our present investigation. Under the assumption that the instability will be present also in the non-linear equations, we may conclude that the very long waves will be unstable in a frictionless and adiabatic atmosphere.

6. Conclusions

The comparison between the different models treated in this paper shows that the effect of the variable static stability is to shift the wavelength of maximum instability toward shorter waves. In the case of the primitive equations we find furthermore that the waves are unstable only between certain limits of the vertical windshear for a given value of the wavelength. Outside these limits the waves are stable.

Relatively small differences are found in the amplification rate of unstable waves in models with the same variation of the static stability, if the Richardson number is large. The differences in the amplification rate increases when the Richardson number decreases.

In the models in which the static stability is allowed to vary we are able to determine the distribution of this quantity in the unstable baroclinic wave. It turns out that the stratification is more stable than the average between the ridge and the trough in the geopotential and less stable between the trough and the ridge, looking downstream. The variation of the static stability is about 20% of the average value.

The meridional component of the ageostrophic wind can be computed in the models which are based upon the primitive equations. We find that the meridional wind component is super geostrophic in the ridge of the geopotential at the upper level, but subgeostrophic in the upper level trough, while the opposite is the case at the lower level. It is furthermore found that the ageostrophic component is a larger percentage of the total meridional wind component at the lower level than at the upper. The ageostrophic wind is about 20% of the total wind at the lower level.

In the model based upon the primitive equations and with variable static stability we find a separate region of baroclinic instability for very long waves. The instability is weaker than in the ordinary region of instability with e-folding times of several days. The structure of these unstable waves is such that the waves in the meridional wind and the geopotential at the upper level are almost 180 degrees out of phase with the corresponding waves at the lower level. Such a structure is very dissimilar to the structure of the very long waves observed in the atmosphere, where we find a much smaller slope. It is possible that the slope which we find in the frictionless and adiabatic model will be greatly modified if friction were included in the model. We can therefore not conclude that the instability which we have found is a result of the simplified model and is unrelated to phenomena in the real atmosphere, but further investigations are necessary to establish the true nature of this instability.

7. Acknowledgements

The author wishes to thank Mr. David L. Kitts who coded and supervised all calculations in connection with this paper.

APPENDIX

It is instructive to consider the types of wave solutions which are possible in the models which have been considered in this paper. This information is most easily obtained from the most general model. The linear equations for this model are written in the system (4.1). The different types of wave solutions can be obtained as special cases of the general system (4.1).

The *inertia waves* can be obtained as solutions of (4.1) in the special case where $U' = \beta = \sigma_0 = 0$, but $f_0 \neq 0$. The equation for the phase-speed is in this case

$$\xi^3\left(\xi^2 - \frac{f_0^2}{k^2}\right) = 0, \tag{1}$$

which has the triple solution $\xi = 0$, corresponding to $c = U^*$, and the solutions $\xi = \pm f_0/k$ or $c = U^* \pm f_0/k$, which are the speeds of the inertia waves with the period $T = 2\pi/f_0$.

Internal gravity waves are obtained as solutions in the special case where $U' = \beta = f_0 = 0$, but $\sigma_0 \neq 0$. The frequency equation is in this case

$$\xi^3(\xi^2 - R\sigma_0/2^{\varkappa+1}) = 0, \tag{2}$$

with the solutions $\xi = 0$, $c = U^*$ (triple root) and $\xi = \pm(R\sigma_0/2^{\varkappa+1})^{\frac{1}{2}}$; $c = U^* \pm (R\sigma_0/2^{\varkappa+1})^{\frac{1}{2}}$.

A combination of the two types of solutions are obtained if we make the assumption that $U' = \beta = 0$, but $f_0 \neq 0$ and $\sigma_0 \neq 0$. In this case the frequency equation is

$$\xi^3\left(\xi^2 - \frac{f_0^2}{k^2} - \frac{R\sigma_0}{2^{\varkappa+1}}\right) = 0, \tag{3}$$

with the solutions $\xi = 0$ (triple root) and $\xi = \pm (f_0^2/k^2 + R\sigma_0/2^{\varkappa+1})^{\frac{1}{2}}$, where the last roots give the speed of the inertia-gravity waves.

An investigation of the system (3.1) shows that it has the same roots in the special cases mentioned above except that the root $\xi = 0$ now is only a double root.

The roots which we have obtained as solutions to equations (3.3) and (4.2) are still of the same type as the very special solutions mentioned above, but they are naturally modified by the inclusion of the beta effect and the effects of the vertical windshear. We may therefore still classify the solutions of for example (4.2) as five wave types, three of which correspond to "meteorological" waves and two to inertia-gravity waves. Of the three meteorological waves, one corresponds to the Rossby wave which can be seen by plotting the speed of the wave on a diagram containing a curve for the Rossby speed $c = U^* - \beta/k^2$. The two curves approach each other when k becomes small.

REFERENCES

EADY, E. T., 1949, Long waves and cyclone waves. *Tellus*, Vol. 1, No. 3, pp. 33–52.

GATES, W. L., 1961*a*, Static stability measures in the atmosphere. *J. Met.*, Vol. 18, No. 4, pp. 526–533.

GATES, W. L., 1961*b*, The stability properties and energy transformations of the two-layer model of variable static stability. *Tellus*, Vol. 13, No. 4, pp. 460–472.

GREEN, J. S. A., 1960, A problem in baroclinic stability. *Quart. J. Roy. Met. Soc.*, Vol. 86, No. 368, pp. 237–252.

LORENZ, E. N., 1960, Energy and numerical weather prediction. *Tellus*, Vol. 12, No. 4, pp. 364–374.

PHILLIPS, N. A., 1954, Energy transformations and meridional circulations associated with simple baroclinic waves in a two-level, quasi-geostrophic model. *Tellus*, Vol. 6, No. 3, pp. 273–287.

WIIN-NIELSEN, A., 1961*a*, On the distribution of temperature relative to height in stationary, planetary waves. *Tellus*, Vol. 13, No. 2, pp. 127–139.

WIIN-NIELSEN, A., 1961*b*, A preliminary study of the dynamics of transient, planetary waves in the atmosphere. *Tellus*, Vol. 13, No. 3, pp. 320–333.